Cylindrical multiwire proportional chambers in physics experiments at JINR and PSI

N. P. Kravchuk
Joint Institute for Nuclear Research, Dubna

Fiz. Elem. Chastits At. Yadra **25**, 1244–1278 (September–October 1994)

This review describes the use of cylindrical multiwire proportional chambers in experiments on rare and forbidden processes in elementary particle physics. The features of several versions of coordinate detectors with cylindrical geometry are described. The basic operating principles of a classical cylindrical multiwire proportional chamber are described. The advantages and disadvantages of various methods of determining event coordinates are reviewed. Special attention is paid to the fundamental problems arising in the operation of cylindrical multiwire proportional chambers with cylindrical geometry and the difficulties associated with using ones containing a small amount of matter. The requirements imposed by experimental goals on coordinate gas-filled detectors are given. The advantages and examples of the use of cylindrical multiwire proportional chambers in actual studies of rare decays of elementary particles using high-intensity beams in the ARES (JINR) and SINDRUM (PSI) spectrometers are described. The parameters and basic characteristics of the various types of cylindrical multiwire proportional chamber forming a fundamental component of the detection systems of these spectrometers are given.

1. INTRODUCTION

The achievements of elementary particle physics are to a large extent related to advances in experimental techniques. This is true both of experiments at ever higher energies, and, in a different direction, precision experiments with very large statistics in energy ranges which have been studied previously. Precision experiments to study rare processes and seek forbidden ones will continue to supply fundamental knowledge about particle physics. New information on processes occurring with probabilities below 10^{-12} can be obtained in experiments performed in high-intensity beams using wide-aperature detection systems with good temporal and spatial resolution. The development of the technique of multiwire gas-filled counters and advances in electronics have led to the construction of detection systems which are capable of handling these problems.

Multiwire proportional chambers and drift chambers have become very widespread in physics experiments.[1–4] The present review deals with proportional chambers. In this operating regime a chamber possesses a number of attractive features:

sufficiently high temporal and spatial resolution;
small dead time allowing efficient operation at large loads;
the possibility of incorporation into trigger systems and preliminary information-readout systems;
representation of data in a form convenient for automated operation;
the ability to operate in a magnetic field;
fairly simple construction, so that the requirements of a specific experiment can be taken into account.

It is precisely the last feature, flexibility in construction, which makes it possible to create cylindrical multiwire proportional chambers surrounding the region where the beam interacts with the target, so that detection in a solid angle of nearly 4π steradians becomes possible. Most modern detection systems, particularly those used in colliding beams or in the study of rare decays, have at least a central region of cylindrical geometry which can be composed of several types of detector, including proportional chambers. The information obtained by these detectors is used to spatially reconstruct an event: the event vertex and the charged-particle trajectories are reconstructed. Proportional chambers are rather fast detectors, and so they are incorporated into the logic of the detector trigger and preliminary information-readout systems.

Gas-filled detectors can operate in a magnetic field, and so the central part of a detector is often located inside a magnet. This makes it possible to measure the sign of the particle charge and the particle momentum from the curvature of the trajectory of a charged particle in a magnetic field. Magnets of solenoidal form are usually used, and a detection system of cylindrical geometry makes the most rational use of the working space inside the magnet.

Another advantage of cylindrical geometry, the isotropy of various features in the plane perpendicular to the cylinder axis, allows the construction of simple and convenient systems for information readout and processing and the simplification and integration of the trigger logic of the detector and the preliminary information-filtering system.

Thus, cylindrical geometry of a chamber ensures the following:

1. A solid angle of detection close to 4π steradians;
2. Optimal use of the working volume of the magnet;
3. Isotropy of characteristics in the angle in the plane perpendicular to the chamber axis.

Several versions of detection systems of cylindrical geometry

In modern detection systems cylindrical structures are created from counters operating on various principles and in

 1063-7796/94/050526-16$10.00

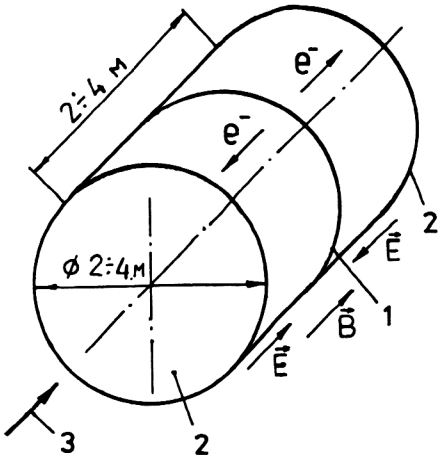

FIG. 1. Schematic depiction of a time projection chamber. *1*—high-voltage electrode; *2*—end two-coordinate gas-discharge chambers; *3*—beam.

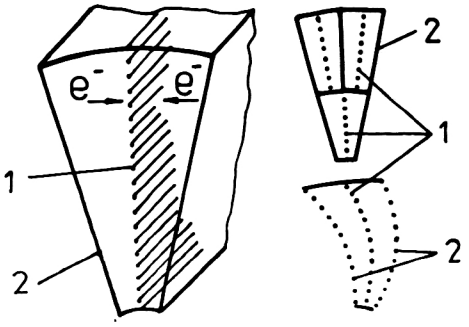

FIG. 2. Schematic depiction of different variants of cells of a JET-type drift chamber. *1*—signal wires; *2*—field-forming electrodes.

various modes: scintillation counters, microstrip semiconductor detectors, microstrip gas-discharge detectors, and various other types of gas-filled detectors.

Before turning to the detailed study of cylindrical multiwire proportional chambers (CMPCs), let us briefly discuss a group of cylindrical detection systems based on gas-filled detectors. Most of these examples can rather be viewed as ways of filling a cylindrical volume, but they are very close in their operating principle and characteristics to proportional chambers, so it is worth listing them and mentioning their most obvious advantages and disadvantages.

The time projection chamber (TPC). Such chambers are used, for example, in the DELPHI, TOPAZ, and ALEPH detectors (Refs. 5, 6, and 7). The main task of detectors of this type is three-dimensional event reconstruction. The TPC is a refined ionization chamber of large size. As a rule, it is a cylindrical vessel (Fig. 1) with a volume of several cubic meters filled with a working gas or mixture of gases. The entire cylindrical vessel is usually placed inside a solenoidal magnet producing a magnetic field parallel to the axis. A system of electrodes located outside the sensitive volume of the chamber produces an axially symmetric electric field inside the cylinder in which electrons produced in the gas along the path of a charged particle drift to the cylinder ends. Gas-discharge chambers for recording two event coordinates are located on these ends. The coordinate along the cylinder axis is determined from the time for the electrons to drift to the ends. It is the large drift distance which gives rise to the main disadvantages of the TPC.

Time projection chambers possess record "transparency," since the sensitive volume of the chamber contains only the working gas, which can also simultaneously serve as the target.

Pictorial or jet drift chambers. These are used in the JADE, OPAL, and H1 detectors (Refs. 8, 9, and 10). Chambers of this type are used in experiments with a high multiplicity of recorded events, when there are 200 or more tracks and their density is high. The cylindrical sensitive volume of such detectors is divided into individual sectors like sections of an orange (Fig. 2). In each sector electrodes placed parallel to the cylinder axis produce an electric field which ensures the azimuthal drift of electrons to the sensitive middle electrode. Each track is recorded at 40–200 points. Owing to the discreteness in the azimuthal direction the electron drift length does not exceed 100 mm, which improves such detector parameters as the speed of response and the spatial resolution. By using gases with low electron drift velocity it is possible to improve the spatial resolution of the detector, though at the expense of worsening the time characteristics.

Dense filling of the cylindrical volume with drift cells. Such constructions have been realized in the ARGUS, HRS, and VENUS detectors (Refs. 11, 12, and 13). The field-forming and signal wires are attached to the cylinder ends and arranged axially in a certain order such that each signal wire is surrounded by field-forming wires (Fig. 3). The usual dimensions of the drift cell in such chambers are $l<10$ mm. A structure this fine-grained leads to improvement in the detector characteristics, and the fact that all the drift cells are identical is convenient for measuring ionization energy losses. The large number of wires in such constructions means that breakage of one of them is rather probable, and this puts the entire chamber out of operation.

This disadvantage is absent in the case of *filling of the cylindrical volume by individual counters*, for example, "straws," as in the MARK III, HRS, and MAC detectors (Refs. 14, 15, and 16). In Fig. 4 we show the arrangement of straws in the MAC detector. The straws usually have a diameter of 5–8 mm and a length of 400–800 mm and are made of thin (30–100 μm) mylar covered with a layer of conducting material. The anode wire is located at the center. Each such counter has its own voltage source and gas sys-

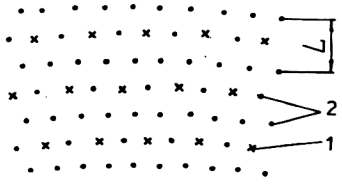

FIG. 3. Example of wire arrangement in the dense filling of a cylindrical space with drift cells. *1*—signal wires; *2*—field-forming wires.

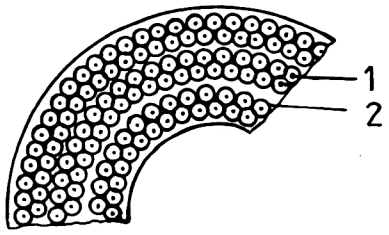

FIG. 4. Example of filling of a cylindrical space with discrete counters. *1*—signal (anode) wire; *2*—cathode.

tem, so that there is little cross-talk and damage to one counter has no effect on the operation of the detector as a whole.

Attempts have been made to design structures which are nearly cylindrical, by *winding wires on support elements located along the axis of a cylinder*. In the chambers of the DMI detector[17] the wires are supported by fiberglass threads. The construction of the Z chamber of the H1 detector (Ref. 18) is shown in Fig. 5.

The main problem solved by chambers of this type is that of obtaining coordinate information along the chamber axis. In return for the relative simplicity of obtaining the z coordinate in chambers of this type, one has to deal with the appearance of dead zones where the wires are soldered or zones of lowered sensitivity at the points where the anode wires are in contact with the supporting elements, and also the injection of additional matter into the sensitive zone of the chamber.

The use of flat microstrip semiconductor detectors and charge-coupling devices for creating detector systems with cylindrical geometry has been studied in the reviews of Refs. 19 and 20. Of interest to us are microstrip gas detectors (MGDs) (Refs. 21 and 22). The structure of such a detector is shown in Fig. 6. The base of the detector is a substrate of insulating material with conducting strips attached to it. The front cathode of aluminumized mylar is located at a distance of 3–5 mm from the substrate, and the gap is filled with a gas mixture of the type used in proportional chambers. Potentials at the field-forming electrodes (positions 2, 3, and 4 in Fig. 6) ensure a gas multiplication of $\sim 10^4$ at the anode

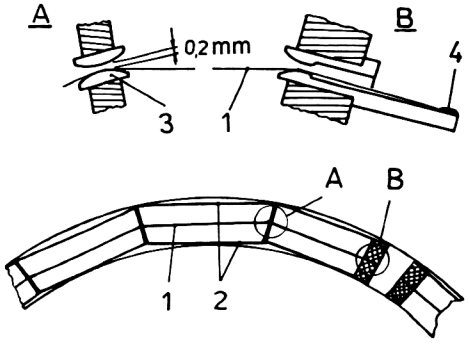

FIG. 5. Construction of a pseudo-cylindrical chamber with supports. *1*—signal wire; *2*—field-forming wires; *3*—supporting element; *4*—points where wires are soldered.

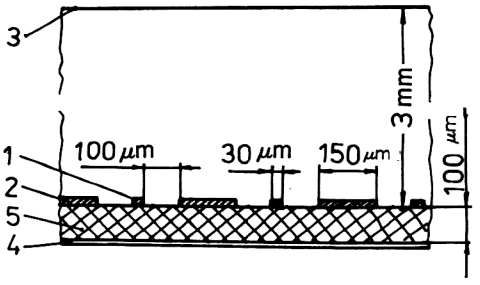

FIG. 6. Transverse cross section through a microstrip gas-discharge detector. *1*—anode strips; *2*—blocking (grounded) cathode strips; *3*—front (drift) cathode made of aluminumized mylar; *4*—rear cathode; *5*—substrate.

strips. The load characteristics of MGDs are better than those of ordinary gas-discharge detectors, and their spatial resolution is better than that of microstrip semiconductor detectors. They have the highest sensitivity.[23]

The construction of MGDs using thin (Kapton, Tedlar of thickness ~ 100 μm) flexible films as the substrate[24] naturally led to the creation of MGDs with cylindrical geometry. This is a very promising development, but so far the first chamber of this type[25] has a diameter of 20 mm and a length of 80 mm for a "thickness" of 10^{-3} radiation lengths.

2. CYLINDRICAL MULTIWIRE PROPORTIONAL CHAMBERS OF CLASSICAL CONSTRUCTION

2.1. Operating principles

The classical cylindrical multiwire proportional chamber (CMPC) is shown in Fig. 7. The anode wires are located along the cylinder axis between two coaxial cylindrical cathodes. The cathodes are made of wire or in the form of solid cylinders. The chambers are filled with a gas mixture based on a gas in which electron capture is absent (usually argon) plus various additions with quenching properties and which prevent secondary electron emission from the cathodes (carbon dioxide, isobutane, methane, and so on).

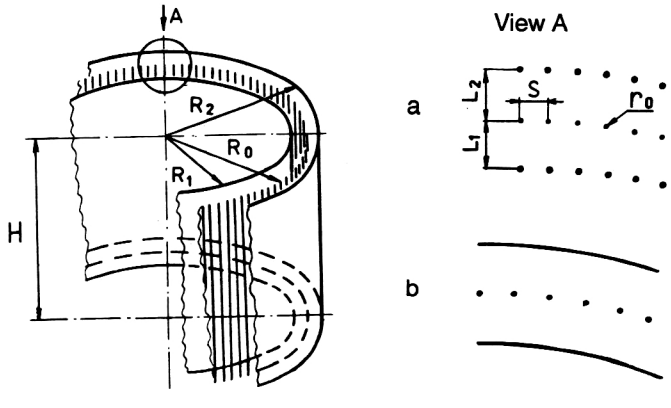

FIG. 7. Schematic depiction of a cylindrical multiwire proportional chamber. (a) Version with wire cathodes; (b) version with solid cathodes. R_0 is the radius of the anode layer of wires; R_1 and R_2 are the radii of the inner and outer cathodes; H is the chamber height; L_1 and L_2 are the anode–cathode distance; S is the spacing of the anode wires; r_0 is the radius of the anode wires.

The equipotentials of the electric field near a thin anode wire have the shape of cylinders with the wire itself as the axis. As for a cylindrical counter,[1)] the electric field strength E near the anode wires is

$$E=2q/r_0,$$

where q is the charge per unit length of the wire and r_0 is the wire radius.

The electrons produced in the gas of the chamber after the passage of a particle drift in the electric field to the anode. Near the anode they move in a region with constantly increasing electric field strength. At some distance the electrons begin to undergo inelastic collisions, forming electron cascades. The gas multiplication factor can be written as[26]

$$A=\exp\sqrt{2aN}\ F(r_0)\sqrt{V_0}[\sqrt{V_0/V'}-1],$$

where V_0 is the potential of the applied external field, V' is the threshold potential at which inelastic collisions begin to occur near the surface of the wire; r_0 is the radius of the anode wire; N is the concentration of atoms of the gas in cm^{-1}; a is the rate of growth of the ionization cross section as a function of energy, and

$$F(r_0)=[(\pi L/S)-\ln(2\pi r_0/S)]^{-1/2},$$

where $L=L_1=L_2$ is the distance between the cathodes and the anode, and S is the distance between the anode wires.

To produce a cascade giving a gas multiplication factor of $\sim 10^6$ an electron must travel a distance of 10–20 mean free paths (~ 20 μm for the gases used). The gas multiplication occurs in a small region near the anode wires, and in the rest of the space the electrons simply drift to the anode. The time for this drift determines the time characteristics of the chamber. In the gases ordinarily used for proportional chambers the electron drift velocity is 0.03–0.1 mm/nsec (at normal pressure). In the case of tracks passing between anode wires ($S=2$ mm) the resolution time of the chamber is ~ 20 nsec.

The spatial resolution of proportional chambers with information readout from each anode wire is mainly determined by the distance between wires S. The accuracy of determining the coordinates of a particle crossing the chamber perpendicular to the electrodes is $\sim S/3$. This corresponds to the standard deviation of a rectangular distribution with width S and has been confirmed in studies using several proportional chambers with reconstruction of a straight track using three chambers.

The distribution of the potentials, fields, and charges in the CMPC for $R_0 \gg R_2-R_1$ is analogous to the corresponding distributions in a planar chamber. In the case of chambers with $L_1=L_2=L>S\gg r_0$, the real part of the potential V is (Ref. 27)

$$V=q\left\{\left(\frac{2\pi L}{S}\right)-\ln\left[4\ \sin^2\left(\frac{\pi x}{S}\right)+4\ \text{sh}^2\left(\frac{\pi y}{S}\right)\right]\right\},$$

where

$$q=\frac{V_0}{2[\pi L/S-\ln(2\pi r_0/S)]}.$$

If an operating potential of ~ 3.6 kV is supplied to a chamber with $L=6$ mm, $S=2$ mm, and $r_0=0.01$ mm, the electric field strength near the anode wires is $\sim 4\times 10^5$ V/cm, and the unit capacitance of the anode wire relative to the high-voltage electrodes is 4 pF/m. The actual shape of the signal is determined by the total capacitance of the channel relative to ground (20–100 pF), and the largest contribution to this quantity comes from the connecting cable and the input capacitance of the preamplifier.

For a gas multiplication factor of $\sim 10^6$ the height of the pulses from the anode wires (the load for $R=1$ kΩ and $C=15$ pF) is several millivolts. A signal of opposite sign but smaller amplitude is induced simultaneously at the cathode surfaces. The signal from the cathodes can be increased by decreasing the anode–cathode gap. For a gap of less than 2 mm the detection efficiency decreases owing to an insufficient number of primary electrons produced (in the gases commonly used). The detection efficiency is defined at

$$\eta=1-e^{-nl},$$

where n is the primary unit ionization for the gas which is used and l is the distance from which the electrons are collected.

It should be noted that the use of gases with larger primary ionization and decrease of the anode–cathode gap allows improvement of the time characteristics of the chamber, but does not improve the chamber "transparency," since such gases have higher density and atomic number Z.

The geometrical parameters of the chamber and especially the variations in them unavoidable in real chambers strongly affect the chamber operation. The greatest effect on the magnitude of the signal from the chamber comes from nonuniformity in the spacing of the anode wires. A variation of $\Delta S=0.1$ mm induces a change of the charge at the adjacent wires of $\Delta q/q=8\%$. A shift of the anode wire toward the cathode has a much smaller effect. Such a radial shift of a wire by 0.1 mm includes a change of the charge at it of $\Delta q/q<0.2\%$.

These and several other aspects of the operation of multiwire proportional chambers have been studied in more detail in Refs. 1, 2, 28, and 29.

2.2. Special features of the cylindrical geometry

As shown above, the CMPC does not fundamentally differ from ordinary planar multiwire proportional chambers. The cylindrical geometry affects only the shaping of the electric field around the anode wire.

The efficient, stable operation of multiwire proportional chambers, both planar and cylindrical, greatly depends on the stability of the wires under the action of electrostatic and gravitational forces, on the accuracy of the spatial location of the electrodes in the chamber, and so on. For planar chambers these problems have been discussed in detail in the literature (Refs. 30–33). In cylindrical chambers it is only the electrostatic forces which have a special effect on the stability of the wires. Stable placement of the anode wire ensures that the condition that the surface charge density of the anode wire is the same for any cross section along its diameter is satisfied.

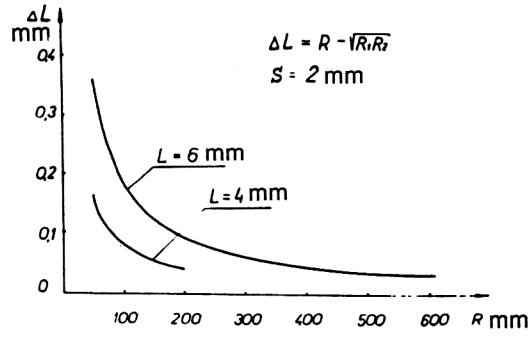

FIG. 8. Needed asymmetry in the placement of the electrodes of a cylindrical chamber to ensure stable positioning of the anode wires as a function of the chamber radius R and the anode–cathode distance L for $V_1=V_2$.

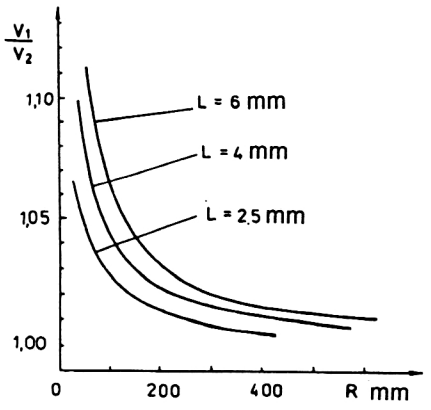

FIG. 9. Ratio of the voltages at the inner (V_1) and outer (V_2) cathodes needed to ensure stability of the anode wires as a function of the chamber radius R and the anode–cathode distance L for $L_1=L_2=L$.

To satisfy this condition in planar chambers it is sufficient to arrange the cathodes symmetrically relative to the anodes (for identical cathode potentials). In cylindrical chambers additional conditions must be met for stability of the anode wires.

To illustrate the appearance of radial instability of the anode wires, let us consider a simplified model of a chamber: a double cylindrical coaxial condenser on the middle cylinder of which are cuts along the cylinder axis. The potential difference between the cylinders is

$$V_1=\frac{q_1}{2\pi\varepsilon}\ln(R_1/R_0),\quad -V_2=\frac{q_2}{2\pi\varepsilon}\ln(R_2/R_0),$$

where R_0, R_1, and R_2 are the cylinder radii ($R_1<R_0<R_2$); V_1 and V_2 are the potential differences between the cylinders with R_1, R_2, and R_0; q_1 and q_2 are the surface charges per unit length of the cylinder; ε is the permittivity of the medium.

To ensure stability of the middle cylinder it is necessary to satisfy the condition

$$q_1=q_2,\quad \text{or}\ \frac{V_1}{\ln(R_1/R_0)}=\frac{V_2}{\ln(R_2/R_0)}.$$

Let $V_1=V_2$. Then stability of the middle cylinder is possible only when

$$R_0^2=R_1\cdot R_2.$$

The same result was obtained in Refs. 34 and 35 in an analysis of the electrostatic forces acting on the wire anode of a cylidrical chamber.

Let us introduce the quantity ΔL characterizing the asymmetry of the chamber necessary to obtain stable positioning of the anode wires:

$$\Delta L=(R_1+R_2)/2-\sqrt{R_1\cdot R_2}.$$

The dependence of ΔL on $R=(R_1+R_2)/2$ is shown in Fig. 8.

We see that for a chamber with $R>250$ mm the correction ΔL is smaller than the actual accuracy with which individual details of the chamber are constructed and so one usually takes $L_1=L_2$.

The condition of stability of the anode wires in a cylindrical chamber ($q_1=q_2$) can also be met by changing the potential at one of the cathodes keeping the distance between the electrodes fixed, $L=R_2-R_0=R_0-R_1$, when $R^2\neq R_1\cdot R_2$:

$$V_1/V_2=\frac{\ln[R_0/(R_0-L)]}{\ln[(R_0+L)/R_0]}.$$

The potential ratio V_1/V_2 as a function of the chamber radius for different L is shown in Fig. 9. We see from this figure that for chambers with typical values of the parameters and radius greater than 50 mm, for $\Delta L=0$ stability of the anode wires is ensured for $V_1/V_2\leq 1.05$. Taking into account the operating potentials of the chambers, this corresponds to a potential difference between the inner and outer cathodes of <100 V.

Therefore, in practice there are two methods of compensating for the instability of the anode wires associated with cylindrical geometry: variation of the geometrical parameters (the anode–cathode gaps L_1 and L_2) or variation of the cathode potentials (V_1 and V_2).

2.3. Information readout

The most basic and simple method of determining the event coordinates when using planar multiwire chambers is by arranging two layers of wires at some relative angle and determining the event coordinates from the numbers of the wires that are triggered. In the CMPC the possibilities of spatial orientation of the wires are limited. Freely strung wires in a cylindrical chamber can run only along the cylinder axis (or at a small angle to it in hyperbolic chambers). In the CMPC the two event coordinates are determined by the chamber radius and the number of the triggered wire. The event coordinate along the chamber axis (z) can be determined in several ways:

1. From the induced signals on a cathode split up into separate zones;[36,37]

2. From comparison of the signals from two layers of wires arranged at different angles;[38,39]

3. From analysis of the arrival time of induced signals at the ends of special delay lines placed parallel to the anode wires;[40,41]

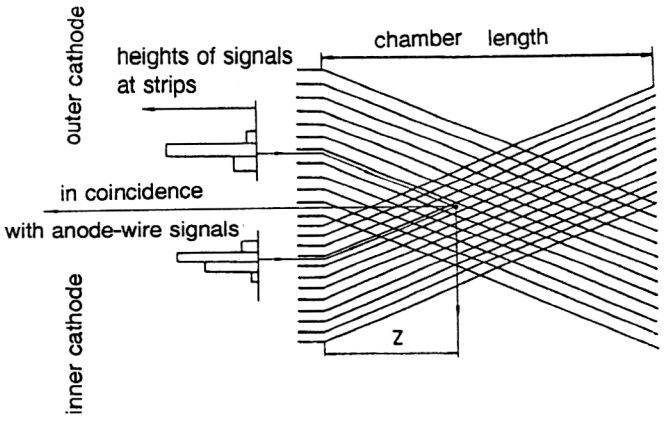

FIG. 10. Illustration of the principle of determining the coordinate along the chamber axis (z).

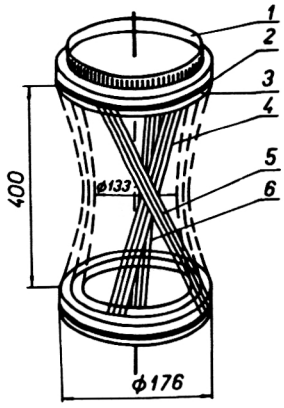

13p

FIG. 11. Sketch of a hyperbolic chamber. *1*—printed circuit board for soldering the anode wires; *2*—band for soldering the cathode wires; *3*—flange; *4*—anode; *5*—outer cathode; *6*—inner cathode.

4. From analysis of the ratio of the signals arriving at the ends of an anode wire possessing large resistence.[42,43]

The *first method* of determining the z coordinate from the signals induced at the helical conducting strips into which the cathodes are divided is used most often in the CMPC. The principle of determining the z coordinate is seen from Fig. 10, where for clarity the cylindrical cathodes with strips are shown unwound.

The track coordinates (the z coordinate and the azimuthal coordinate) are determined using the known slope angles of the strips and the other parameters. The accuracy of determining the coordinate in this way depends on the distance between the strips S, the angle of slope of the strips relative to the cylinder axis α, the accuracy of the geometrical placement of the strips, and the method of processing the signals from the strips. The latter is crucial.

For discrete information readout, for example, using the number of the strip with the maximum signal height, the z coordinate is determined with accuracy

$$\sigma_z = S/12^{1/2} \cdot \sin \alpha .$$

Decrease of the spacing S leads to an increase of the needed number of electronics channels. The increase of the angle α is limited by the condition of uniqueness in determining the z coordinate: the strip must make less than one turn on the cylinder.

When the z coordinate is measured using the center of gravity of the amplitude of the signal induced at the cathode strips the accuracy is mainly determined by the quality of the electronics: the accuracy of the pulse height–code transformers. When a sufficiently large signal is induced on 3–5 strips (strip spacing approximately equal to the anode–cathode distance) the accuracy which can be attained is <40 μm (Ref. 44).

Variants in which the strips are arranged perpendicular to the cylinder axis ($\alpha=90°$) or where the cathodes are divided into pads can be used to obtain rapid information about the z coordinate (for discrete signal readout). However, these are rarely used owing to difficulties with information readout from strips or pads. In these cases the contacts are located on the surface of the cathode cylinders in the working zone of the chamber, rather than on the flanges, as in the case of slanted strips. In addition, the variant with pads requires a large number of electronics channels to obtain comparable accuracy.

The *second method* of determining the z coordinate is used in cylindrical chambers whose wires are wound on a supporting cylinder[38] and in hyperbolic chambers.[39,45] In this case discrete information from the anode wires is used, and the coordinate accuracy, like in the variant with cathode strips, is determined by the slope angle of the wires and the distance between them.

In a hyperbolic multiwire proportional chamber[45] (Fig. 11) the wires are stretched at an angle to the axis and their envelopes form coaxially positioned, hyperbolic surfaces of electrodes (unipolar hyperboloids of rotation). The use of such a chamber in conjunction with a cylindrical or hyperbolic chamber (having a different angle of slope of the anode wires) makes it possible to obtain complete information about the event coordinates from the numbers of the triggered anode wires. It is possible to manage without one hyperbolic chamber by working with induced signals from individual cathode wires positioned at a different angle relative to the inner and outer cathodes.

The main advantage of a hyperbolic chamber is the possibility of measuring the z coordinate for a small amount of matter in the working zone. Among its defects are the low accuracy of determining the z coordinate owing to the small slope angle of the wires. The slope angle can be increased by decreasing the diameter of the chamber at half-height and accordingly increasing the space occupied by the chamber, especially for chambers with small (compared to the height) diameter.

The *third method* of obtaining the z coordinate is to place a delay line next to the cathode, or to connect the cathode itself to a delay line. The signal induced on the delay line propagates to its two ends with known velocity. The coordinate of the electron cascade at the anode wire is determined from the difference between the arrival times of the signal at the wire and at the end of the delay line.

The spatial resolution can be improved by using longer

delays, but this means using a larger amount of matter and so the "transparency" of the chamber is worsened.

The *fourth method* of obtaining the z coordinate, the current-splitting method, is based on measurement of the currents at the two ends of the anode wire. The currents are split according to the resistances of the wire segments in either side of the point where the electron cascade develops. The measurement error is decreased by using anode wires made of materials with high resistance. The accuracy of measuring the z coordinate in this way is usually not very high: $\Delta z/z \sim 1\%$.

The last two methods of obtaining the second coordinate do not have any special features associated with the cylindrical geometry of the chamber, and so we have not considered them in much detail.

2.4. Technical difficulties in the design and use of CMPCs

The complexity of creating any surface of second order, including a cylindrical one, compared to a flat surface is obvious. It is important to stress the basic problems which arise in "curving" a planar chamber to make it fully cylindrical:

There are no flanges along one direction, and so there is no support (unless an auxiliary one is introduced) for attaching and holding under tension the wires or films in this direction. There are fewer possible arrangements of contact connectors, electronics, etc.

The *construction of cylindrical chambers is considerably more complicated* than that of planar ones. The uniform elements (anode and cathode electrodes, shielding windows, etc.) of planar chambers can be built independently of each other and then connected to form chambers or blocks of chambers. The elements of a cylindrical chamber are not uniform in some parameters such as the diameter, and the construction of such a chamber is similar to the step-by-step assembly of a "matryoshka," a nested set of dolls.

The construction of *separable cylindrical chambers* involves great difficulties. It can become necessary to disassemble the chamber when, for example, repair is needed after breakage of one of the anode wires. The probability of such a breakage is significant because the number of wires in such a chamber ranges from a hundred to several thousand and their diameters are 15–25 μm.

In the case of a planar chamber there are several ways to extract an inner plane from the stack. The assembly and disassembly of coaxially arranged cylinders is possible only along the common axis of the cylinder. The situation is complicated by the fact that some of the elements in cylindrical multiwire chambers by themselves have an unstable state. For example, an anode electrode extracted from a planar chamber is a rigid frame strung with wires. The anode electrode of a cylindrical chamber is composed of two rings connected by thin wires, and it is difficult for it to exist independently, without some support.

The wires of an anode electrode of a cylindrical chamber are usually attached to the flanges of the inner cathode held by the supporting cylinder. If the outer cathode does not have its own supporting cylinder, the chamber is not separable, since the number of independent parts into which the chamber can be divided is equal to the number of supporting elements in it. It has proved possible in practice to construct only semi-separable CMPCs which can be divided into two parts: the inner cathode with the anode and the outer cathode.

Difficulties in constructing CMPCs containing a small amount of matter. In the case of planar chambers the supporting flanges are located along the periphery of the working zone of the chamber, and the problem of "transparency" does not arise. In the case of a cylindrical chamber the tracks of the recorded particles usually start at the common axis and intersect the supporting cylinders to which the flanges of the chamber are attached. The "transparency" of a cylindrical chamber can be improved by decreasing the amount of matter in the supporting cylinders or by introducing auxiliary supporting elements. Cylindrical chambers are often used in assemblies of several coaxially arranged chambers, and the supporting element in such assemblies must be extended beyond the dimensions of the outside of the chamber. An example of such a construction used in the ARES spectrometer will be considered below.

The difficulties in assembling and disassembling a single CMPC and connecting its elements together also arise in the case of a set of several coaxially arranged cylindrical chambers, but at a larger scale.

Another special feature of CMPCs is that they are usually located in the restricted working space of a magnet and this space must be utilized as efficiently as possible. Therefore, the elements of which the chamber is constructed must be as small as possible.

2.5. Some of the special requirements on CMPCs

We shall not dwell on such common requirements imposed on coordinate detectors as accuracy of coordinate measurement, good time characteristics, high efficiency, and reliability. We only stress the great importance of the last requirement for cylindrical chambers in particular. High reliability is the necessary condition for using chambers in a complex setup, when replacement of the chamber involves a great deal of time and data-collection sessions are of long duration.

The difficulty of building a CMPC containing a small amount of matter was mentioned above. The importance of satisfying this condition should be noted.

The accuracy of the spatial reconstruction of an event, the ability to detect particles of low energy, the accuracy of measuring the momentum of a charged particle from its trajectory in a magnetic field, and the minimum value that can be measured are all directly related to the chamber "transparency," i.e., to the energy losses of particles in the material of the chamber and to their multiple scattering.

For singly charged particles of energy in the range 10–150 MeV the energy losses are the sum of the losses to ionization and excitation of nuclei and to bremsstrahlung. The energy losses to ionization and excitation of nuclei amount to (1.5–3) MeV·cm^2/g and depend little on the atomic number Z of the material of the medium or on the particle energy. The energy losses to bremsstrahlung (radiation losses) can be determined from the expression[46]

$$\frac{(dE/dx)_{\text{rad}}}{(dE/dx)_{\text{ion}}} \sim \frac{EZ}{800},$$

where E is the particle kinetic energy in MeV.

Therefore, the change of radius of the trajectory of charged particles in a magnetic field due to energy losses can be taken into account if the characteristics of the particles and the medium are known. An additional uncertainty arises owing to the impossibility of precisely determining the trajectory of a particle in an inhomogeneous medium. The large number of layers of wires with spacing ~2 mm makes the probability of hitting a wire rather high, and the total energy loss of an electron ($E_e = 50$ MeV) in passing through the center of a wire (tungsten, $\Phi = 0.02$ mm or bronze, $\Phi = 0.1$ mm) is ~0.5 MeV.

Analogous difficulties arise when taking into account particle multiple scattering, which is random in nature. A charged particle passing through a layer of matter undergoes multiple Coulomb scatterings at small angles. A measure of the scattering is the rms scattering angle θ (Ref. 47):

$$\theta = \frac{t}{pj} K(j,q,t).$$

In this expression the particle is characterized by its charge q, its momentum p, and its relative velocity j, and the medium is characterized by its radiation length t. The quantity $K(j,q,t)$, the so-called scattering constant, is a weak, nearly logarithmic function of these parameters. For a qualitative analysis of the dependence of the scattering of singly charged particles on the parameters characterizing the particle and the medium, the expression for the scattering angle can be written as

$$\theta \simeq \frac{Z(l\rho)^{1/2}}{pj},$$

where l is the length of the trajectory, ρ is the density of the medium, and the other notation is as above.

To reconstruct the complete picture of events involving gamma quanta it is necessary to detect the gamma quanta. They are not detected directly by a proportional chamber, but they can be recorded using the ionization effect generated by secondary charged particles. Gamma quanta passing through a medium can be absorbed by the atoms of the medium (the photoeffect), they can undergo scattering on the atomic electrons (Compton scattering), and they can undergo conversion into electron–positron pairs in the electric field of a nucleus. For low gamma energies the dominant mechanism for interaction with matter is the photoeffect. At intermediate energies the Compton effect dominates. At gamma energies of $E_\gamma \geqslant 2m_e c^2 = 1.022$ MeV electron–positron pair production becomes possible, and at higher gamma energies this is the dominant mechanism for their interaction with matter. The total cross section for these processes is

$$\sigma = \sigma_{\text{ph}} + \sigma_{\text{C}} + \sigma_{\text{p}},$$

where $\sigma_{\text{ph}} \sim Z^5/E_\gamma^{7/2}$ is the photoeffect cross section, $\sigma_{\text{C}} \sim Z/E_\gamma$ is the cross section for the Compton effect, and $\sigma_{\text{p}} \sim Z^2 \ln 2E_\gamma$ is the cross section for pair production.

Gamma quanta are usually detected from the production of a conversion electron–positron pair or in a total-absorption calorimeter. In the first method proportional chambers are located behind the gamma converter and record the electron–positron pairs created in the converter. In the second, proportional chambers are located in front of the calorimeter recording gamma quanta. In both of these methods it is necessary to decrease the probability for the gamma quantum to interact with the material in the proportional chamber, since each interaction leads either to the complete disappearance of the quantum or to a significant change in the direction of its motion, and an electron–positron pair or a fast electron can appear. This all complicates the identification of the primary process.

It is clear from the above discussion that it is important to try to decrease the amount of matter in the working volume of the detectors and to use materials with low atomic number Z.

3. EXAMPLES OF THE USE OF CMPCs

Cylindrical proportional chambers have such attractive advantages that all the difficulties discussed above related to the cylindrical geometry do not stop them from being used in experiments. From the time the first CMPCs were constructed (Refs. 38, 48–50) to the present, they have formed an important part of many detectors. As an illustration, in Table I we list a number of detectors in which two or more CMPCs are used and give some of the parameters of these chambers.

Let us discuss some of the experiments in which CMPCs are used in more detail (Table II). These experiments are carried out to test the fundamental laws of physics and to study the most fundamental properties of particles. The different stages of realization of the projects—from completed to planned for the future—attest to the seriousness of this methodological approach to solving the problems in question.

A common feature of all these experiments is that the probabilities for the processes studied or sought are extremely low (from $W \sim 10^{-8}$ to $<10^{-12}$), so they are carried out in beams of high intensity using wide-aperature devices with high spatial and temporal resolution. The detected particles have relatively low energy (<150 MeV), and in the same energy range there are pion and muon decay products, which give the dominant contribution to the background seen in the detectors. As mentioned above in Sec. 2.5, for recording and reconstructing the trajectory of an electron or positron at such energies it is important to use detectors containing a small amount of matter in the working volume, and this matter should have small atomic number.

3.1. The ARES spectrometer (JINR)

Search for the decay $\mu^+ \to e^+ e^+ e^-$ (Ref. 63). Experiments to seek decays of the type $\mu^+ \to e^+ e^+ e^-$, $\mu^+ \to e^+ \gamma$, and the conversions $\mu^- \to e^-$ and $(\mu^+ e^-) \to (\mu^- e^+)$ are one of the most important areas of research in weak-interaction physics. These processes are forbidden in the standard model of the electroweak interaction owing to conservation of muon number, which distinguishes muons from

TABLE I. Examples of the use of cylindrical multiwire proportional chambers in detectors.

Detector, laboratory	Number of chambers	(Useful) chamber dimensions (mm)		Number of singal wires	Amount of matter in the chamber		Reference
		length	radius		(mg/cm^2)	(r.l.)$\times 10^{-3}$	
ASTERIX,ORSAY	2	960–1070	700–870	3608	···	3.2–5.0	[51]
CLEO,CLNS	3	790	108–154	720	500/3*	25/3	[52]
Exp.E68,KEK	4	684	120–215	1060	160	···	[53]
LASS,SLAC	6	1000–870	60–490	3882	110	···	[54]
NA-1,LNF	4	500	30–120	900	48	···	[55]
UA-2,ORSAY	5	800–1800	100–355	2688	···	2.3–2.6	[56]
L3,LEP	2	1068	468–490	2430	···	20/2	[57]
CMD-1,BINP	2	800	306–324	1408	···	24/2	[58]
H-1,DESY (PSI)	2	2190	157–166	960	102.4	1.4	[59]
SINDRUM,PSI	5	360–800	64–320	2890	31–64	0.8–1.8	[60]
SIGMA-AYAKS,JINR	4	760	64–223	512	375	···	[61]
ARES,JINR	18**	360–600	64–520	14016	38/2–180	1.6/2–4.6	[62]

*Indivisible blocks of 3 (2) chambers.
**12 of the 18 chambers have the minimum amount of matter (19 mg/cm^2 per chamber).

electrons and muon neutrinos from electron neutrinos. Some of the theories which have been proposed allow the existence of massive neutrinos, horizontal gauge bosons, preons, or supersymmetric particles, and in them such processes with muon-number violation can occur.

The progress in experimental research in this area has made it possible to judge the correctness of the various theoretical approaches and to contribute to the solution of fundamental problems in modern physics.

Experiments to seek the decay $\mu^+ \to e^+ e^+ e^-$ have simultaneously collected statistics for studying *the weak electromagnetic decay of the pion* $\pi^+ \to e^+ \nu_e e^+ e^-$ (Ref. 64), which allows study of the pion structure, determination of the electromagnetic radius of the pion, and verification of the CVC and PCAC hypotheses. These muon decays are convenient experimentally because they can be efficiently detected and identified from the three charged particles in the final state. An experiment has been carried out at the Laboratory for Nuclear Problems of the JINR in the muon channel of the synchrocyclotron using the magnetic spectrometer ARES (from the Russian for Rare Event Analyzer; Ref. 64).

The general design of the ARES magnetic spectrometer is shown in Fig. 12. The spectrometer consists of a detecting part incorporating CMPCs, scintillation counters, a converter and a target; a magnet producing a uniform magnetic field in the detecting part; a system for triggering the detector; a system for information readout and processing.

The main coordinate detectors of the ARES spectrometer are 18 coaxially arranged CMPCs with a small amount of matter in the working volume.[62,66] Two types of chambers are used: ones which record only the azimuthal coordinate, and two-coordinate ones which record the azimuthal and axial (z) coordinates. The parameters of the CMPCs of the ARES spectrometer are given in Table III. The curly brackets label blocks of two chambers operating as a single one and having a common gas-filled volume. The number of anode wires in the chambers is a multiple of 32 in order to unify the electronics systems. The spacing of the cathode wires in all the chambers (with cathodes of type II) is 2 mm.

The cathodes of the two-coordinate chambers (type I) are made from solid lavsan cylinders and have helical aluminum strips. In Table III we give the number of strips and their slope relative to the cylinder axis. The strips are twisted on the inner and outer cathodes in opposite directions. Processing of the signals induced on the strips gives complete information about the axial and azimuthal coordinates of the particle track. CMPC 1 has an additional third layer of cathode strips on the outer cathode, and the information from these can be used to resolve ambiguities in determining the

TABLE II.

Detector (institute)	Process	Intensity (stoppings/sec.)	Attained (projected) result	Detected particles	Energy per particle (MeV)
ARES (JINR)	$\mu^+ \to e^+ e^+ e^-$	$6 \cdot 10^5$	$W < 10^{-11}$ (1990)	e^+, e^-	< 53
	$\pi^+ \to e^+ e^+ e^- \nu$	$6 \cdot 10^5$	$W < 9.1^{-9}$ 8 events (1990)	e^+, e^-	< 70
	$\pi^+ p \to e^+ e^- n$	$10^5 - 10^6$	(1994–1995)	e^+, e^-	<140
SINDRUM-1 (PSI)	$\mu^+ e^- \to \mu^- e^+$	10^7	$W < 5 \cdot 10^{-9}$ (1993) $W < 10^{-11}$ (1994)	$e^-(e^+)$	< 53
Crystal-sphere (PSI)	$\pi^+ \to \pi^0 e^+ \nu$	$5 \cdot 10^6$	$W \sim 10^{-8}$ improve accuracy from 4% to 0.2% (1994–1995)	e^+	< 4

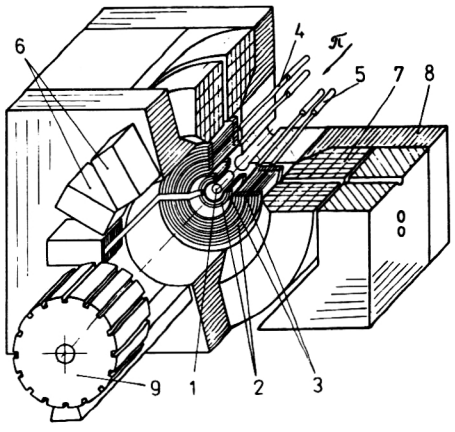

FIG. 12. General view of the ARES spectrometer. *1*—target; *2*—CMPCs 1 through 18; *3*—scintillation counters; *4*—light guides; *5*—photomultipliers; *6*—CMPC electronics; *7*—magnet windings; *8*—magnet yoke; *9*—magnet pole.

coordinate along the chamber axis when recording events with two or more tracks.

There are two classes of chamber according to construction type: self-supporting and extendable. The last column in Table III contains information about the total amount of matter in the chambers. We see that in the self-supporting chambers (1, 2–3, 4, 9, and 13) most of this quantity comes from the supporting cylinders.

High transparency of the detecting region of the spectrometer has been obtained by using mostly (12 out of 18) chambers of the extendable type. The construction of a block made from two extendable chambers (CMPCs 6–7) is shown schematically in Fig. 13. Initially the circular flanges (1) are attached to an internal supporting element (2) in the shape of a cylinder. Wires are stretched between the flanges over the cylindrical form. The wires located at the same diameter form the chamber electrodes (3, 4). At the time the chamber is installed in the operating site the flanges are attached to the structural elements of the common box enclosing the detecting part, and the internal supporting element is removed while maintaining the tension of the wires by the external covering of the box. Only the electrode wires, the working gas, and the lavsan films (5) bounding the gas-filled volume remain inside the detecting region.

This technology has been used to build cylindrical chambers with a record-setting minimum amount of matter in the working volume. In Table IV we give the composition and amount of matter in the block of two extendable chambers (CMPCs 6–7) shown in Fig. 13.

We see that the largest contribution comes from the protective lavsan windows. The total amount of matter in chambers built with this technology can easily be reduced to 5.5 mg/cm^2 per chamber, a value comparable to the contribution from the working mixture of gases. For this it is necessary to decrease the thickness of the lavsan windows to 0.02 mm and to make the cathodes from wire with Φ=0.05 mm and a spacing of 1 mm (Ref. 67).

In all the extendable chambers the spectrometer determines only the azimuthal event coordinate according to the number of the triggered wire.[2)]

Self-supporting two-coordinate chambers have been built. The flanges of such chambers are connected to a thin-walled supporting cylinder, which supports the anode wires under tension. The cathodes are made in the form of solid lavsan cylinders, on the inner surfaces of which are helical conducting strips (Al). The inner cathode is combined with the supporting cylinder, and the outer cathode serves simultaneously as a cover keeping the gas inside. The required accuracy and stability of the cathode and supporting cylinders is ensured by gluing them from several layers of lavsan film cut from a particular pattern.

The chambers operate using a mixture of gases: 82.6% argon (Ar), 17% isobutane (i-C_4H_{10}), and 0.4% freon ($CBrF_3$) at atmospheric pressure with continuous flushing.

The operating potential of the chambers of the ARES spectrometer lies in the range 1.8–3.6 kV. The large spread is due to different anode–cathode gaps, different spacing between anode wires, and different types of cathodes in the chambers. In all the chambers a high negative potential is supplied to the cathode electrodes, and the anode wires are grounded through a resistance (1 $k\Omega$) which is also used for signal readout.

Two-coordinate chambers have been built with two different cathode constructions and schemes for high-voltage supply and information readout. In one case the high voltage is fed to the cathode strips located on the inner side of the lavsan cathode cylinders. The signals induced at the cathode strips are read out through high-voltage blocking capacitors (500 pF) located on the flanges of the chamber.

In part of the chamber the high-voltage cathode electrode is completely isolated from the cathode strips and, consequently, from the readout electronics. The cathodes in such chambers are made in the form of lavsan cylinders with their outer surface coated with a weakly conducting compound based on carbon (~100 $k\Omega$/area). This resistance ensures that a uniform potential can be established at the cathode for high loads (10^3/sec·cm^2) and at the same time ensures sufficient amplitude of the signal induced at the conducting strips located on the outer side of the lavsan cylinder.

In the experiment we have described the average intensity of pion stoppings with subsequent decay $\pi^+ \to \mu^+ \nu$ and muon stoppings in the target was 5.8×10^5 sec^{-1}. During a clean run, 1.15×10^{12} muons decayed in the target. This made it possible to estimate the relative probability for the decay $\mu^+ \to e^+ e^+ e^-$ as $\leqslant 3.6\times10^{-11}$ and to find 8 events of the rare decay $\pi^+ \to e^+ e^+ e^- \nu$.

Only 10 chambers of the charged-particle detector of the spectrometer were used in the experiment. The gamma-quantum detector, which included the converter and the chambers located behind it (CMPCs 13–18), was replaced by an absorber in order to decrease the undesired background. In Fig. 14 we show one of these background events.

The proportional chambers and methods of information processing that were used ensured a spatial resolution of ~1 mm. The use of improved processing techniques[68] made it possible to raise the accuracy by a factor of 1.5. The total

TABLE III. Basic parameters of cylindrical proportional chambers of the ARES spectrometer.

Chamber	Diameter of anode layer (mm)	Number of anode wires	Spacing of anode wires (mm)	Anode–Cathode separation (mm)	Chamber length (wires) (mm)	Type of cathode: I-solid II-wire	Number of Strips			Slope angle of strips (°)			Amount of matter	
							surface 1	surface 2	surface 3	surface 1	surface 2	surface 3	$\times 10^{-2}$ (g/cm^2)	$\times 10^{-4}$ (r.l.)
1	128	192	2.09	2.5	360	I	32	32	16	54.55	−46.51	90	7.1	18.5
2	164	256	2.01	6	400	II	...	...	...	...	...	...	13.8	42.3
3	212	320	2.08	6	400									
4	274	384	2.24	4	500	I	48	48		58.83	−60.87		11.2	28.5
5	319.6	480	2.09	6	500	II	...	...	...	...	...	...	3.8	15.6
6	343.6	512	2.11	6	500									
7	405.5	640	1.99	6	500	II	...	...	...	...	...	...	3.8	15.6
8	429.5	672	2.01	6	500									
9	478.8	768	1.96	4	600	I	96	96		58.78	−59.97		13.6	34.7
10	539.3	768	2.21	6	600	II	...	...	...	...	...	...	3.8	15.6
11	563.3	768	2.30	6	600									
12	629.2	960	2.06	6	600	II	...	...	...	...	...	...	3.5	12.5
13	702.2	1152	1.92	6	600	I	128	128		57.89	−59.12		18.2	46.3
14	758	1152	2.07	6	600	II	...	...	...	...	...	...	3.8	15.6
15	782	1152	2.13	6	600									
16	841.9	1152	2.30	6	600	II	...	...	...	...	...	...	3.8	15.6
17	865.9	1152	2.36	6	600									
18	1038.7	1536	2.12	6	600	II	...	...	...	...	...	...	3.5	12.5
Σ	...	14016	...	...	...	...	...	...	...	...	...	...	89.9	273.3

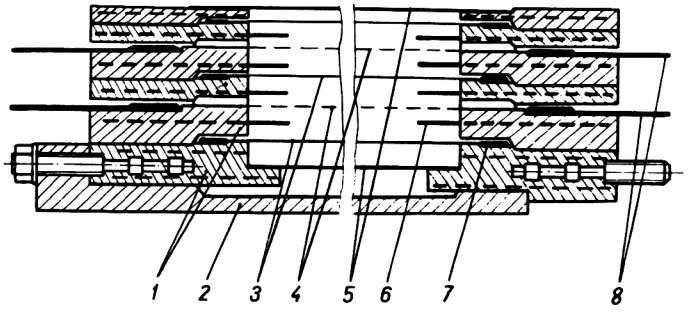

FIG. 13. Cross section of an extendable CMPC (chamber shown on drawing; the axis of rotation runs horizontally, at the bottom). *1*—rings forming the flanges of the chamber; *2*—spacing element; *3*—cathode wires; *4*—anode wires; *5*—shielding and covering envelope; *6*—protective ring; *7*—site to which the cathode wires are soldered; *8*—circuit board for soldering the anode wires.

recording efficiency of the chamber–readout electronics channel was 97% on the average.

The advantages and possibilities of cylindrical geometry and proportional multiwire chambers which are used extensively in the ARES spectrometer are the following:

•The total solid angle for detection is $\sim 0.7 \cdot 4\pi$ steradians, with uniformly good transparency over the entire angle.

•The sensitive region of the detecting part (of diameter 1050 mm) occupies practically the entire working cavity of the magnet, which is cylindrically shaped with a diameter of 1090 mm.

•The CMPCs, being rather fast detectors, were incorporated into the spectrometer triggering system, and the azimuthal symmetry allowed convenient organization of fast trigger logic based on majority coincidence schemes.[69]

•It is the azimuthal symmetry which made it possible to design a simple and flexible algorithm for fast information filtering, making it possible to find events with a given number of tracks of a certain curvature.[70]

•The detection system of the spectrometer has threshold characteristics in the momentum. Charged particles in a uniform magnetic field move along helical paths with radius of curvature.

$$r = P \cdot \sin\theta / 300 \cdot H \cdot Z,$$

where P is the particle momentum in eV/c, Z is the particle charge in units of the electron charge, H is the magnetic field strength in Oe, r is the radius of the helix in cm, and θ is the angle between the vectors **H** and **P**.

All singly charged particles coming from a point target located on the spectrometer axis are completely turned around and are not detected in a chamber with radius r_p if their momentum $P_p < 300 H r_p$. In the ARES spectrometer this is used to create a "magnetic shield" for a gamma-quantum detector.[71]

Inverse pion electroproduction. There are plans to perform an experiment to study inverse pion electroproduction on the nucleon $\pi^+ p \to e^+ e^- n$ using the ARES spectrometer in 1994–1995 (Ref. 72). The experiment is to be performed in the meson channel of the synchrocyclotron of the Laboratory for Nuclear Problems of the JINR at a pion kinetic energy of 50 MeV. Experimental data on this process are completely absent in this energy range, and inverse pion electroproduction on the nucleon is the only source of information about the nucleon form factors in the "near-threshold" region of timelike momenta.

The energy and emission angle of the e^+ and e^- will be recorded by the charged-particle detector (CMPCs 1–12) of the ARES magnetic spectrometer. Changes have been made only in the construction of the block containing CMPCs 2–3, where chamber 2 was replaced by a two-coordinate one. It has been suggested that a hodoscope of neutron counters be placed at the site of the gamma detector (the converter and CMPCs 13–18).

The possibility of studying the rare decay $\pi^+ \to \mu^+ e^+ e^- \nu_\mu$ using the ARES spectrometer is being discussed. The theoretical estimates of the probability for this decay ($\sim 10^{-6}$) disagree by about an order of magnitude. In Ref. 73 it was shown that detection of $(1-5)\times 10^2$ events at a rate of 5×10^5 sec^{-1} is feasible. At present there are indications that a single event has been observed.

3.2. The spectrometer SINDRUM 1 (PSI)

Searches for muonium–antimuonium transitions (Refs. 74 and 75). Muonium–antimuonium transitions ($\mu^+ e^- \to \mu^- e^+$) are forbidden in the standard model of electroweak interactions by the law of muon-number conservation. The importance of carrying out such experiments has been mentioned above in Sec. 3.1. The experiment we shall describe aims to measure the probability of the muonium–antimuonium transition at a level $\sim 10^{-11}$, which is about four orders of magnitude better than that available at present.

The principle of detection of this transition is shown in Fig. 15. The presence of initial muonium atoms is established by the simultaneous detection of an energetic positron

TABLE IV. Data on the matter in a block of two extendable chambers of the ARES spectrometer.

	Material	Number of pieces (wT)	Thickness (mm)	Atomic number Z	Amount of matter mg/cm^2
Shielding windows	lavsan	2	0.1	~7	2×13.9
Cathode	BrB_2	3	Φ=0.1 (spacing 2)	~29	3×3.3
Anode	W(Re) gold-plated	2	Φ=0.02 (spacing 2)	~74	2×0.3
			Combined for both chambers: 38.3		

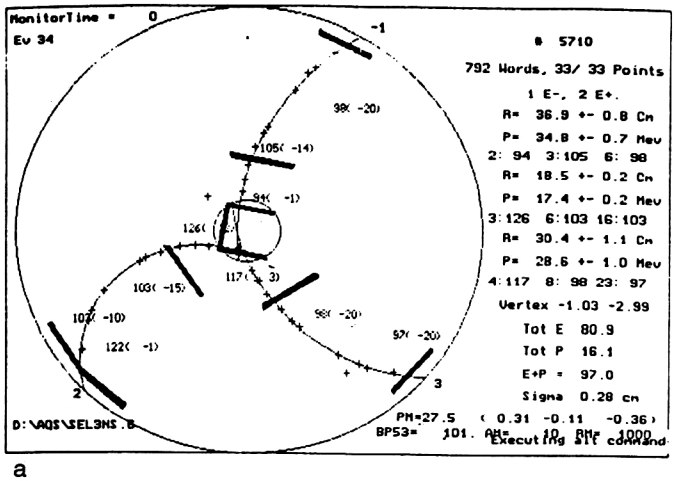

a

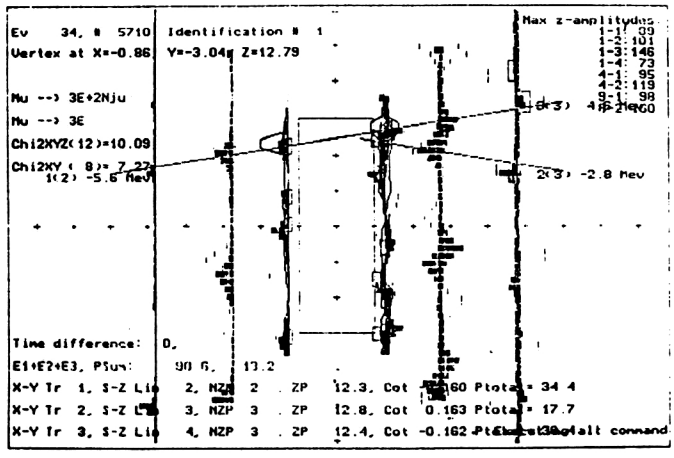

b

FIG. 14. Example of an event reconstruction. (The figure shows auxiliary information, the result of processing the event at various stages of the filtering.) (a) Event in the $R-\varphi$ plane. The initial information for the trigger is the firing of the scintillation counters (short, dark lines) in all three rows of the hodoscope. The tracks are reconstructed using the triggered wires (labeled by crosses) in the 10 chambers. (b) Event in the $R-z$ plane. The tracks are reconstructed using the processed signals from the cathode surfaces of chambers 1, 4, and 9.

from muon decay and a residual low-energy electron. The occurrence of a muonium–antimuonium transition is discovered by detecting an energetic electron and a low-energy positron.

The experiment is shown schematically in Fig. 16.

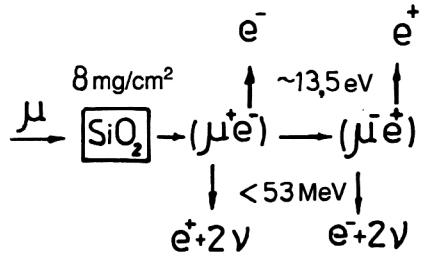

FIG. 15. Principle of detection of the muonium–antimuonium transition.

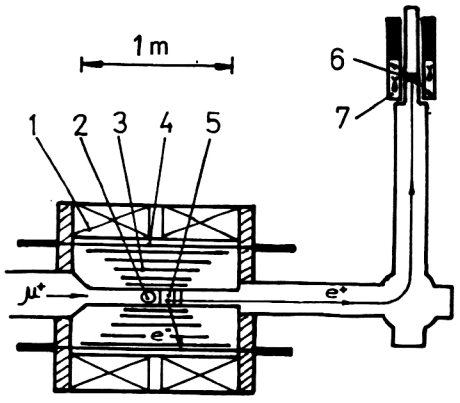

FIG. 16. Schematic depiction of the experimental setup to search for the muonium–antimuonium transition. *1*—magnet; *2*—target; *3*—CMPCs 1 through 5; *4*—scintillation counters; *5*—positron accelerator; *6*—microchannel position-sensitive detector; *7*—gamma-quantum detector.

A beam of surface muons from the PSI cyclotron of intensity $\sim 10^7$ and momentum 19–21 MeV/c is stopped in a fine-grained SiO_2 target. Muonium produced in the target travels into the vacuum region surrounding the target. The muonium–antimuonium transition (if allowed) and antimuonium decay occur in this region.

Electrons from muon decays (with Michel spectrum of energies <53 MeV) are detected by the modernized magnetic spectrometer SINDRUM. This spectrometer has been used successfully earlier to search for and study rare muon and pion decays.[76,77]

In the present experiment the spectrometer is augmented by a special apparatus allowing the detection of the low-energy (~ 13 eV) positron remaining after antimuonium decay. For this the positron is first accelerated to an energy of 10 keV and then transported to the positron detector, where it is also detected in a positron-sensitive microchannel detector. The gamma quanta appearing in the positron-annihilation process are also detected by a hodoscope of 12 scintillation (CsI) total-absorption counters. Information from the positron-sensitive positron detector is used to reconstruct the antimuonium decay point.

The detecting part of the SINDRUM 1 spectrometer is located in a superconducting magnet of the solenoidal type (1 kG). It consists of five coaxially arranged cylindrical multiwire proportional chambers surrounded by a hodoscope of scintillation counters. The total solid angle of detection of the spectrometer is $\sim 0.73 \cdot 4\pi$ steradians. The main parameters of the CMPCs of the spectrometer are given in Table V.

The coordinate along the chamber axis z is measured by chambers 1, 3, and 5 from the signals induced at the cathode strips arranged at an angle of $\pm 45°$. In chamber 1 the strips make two turns on the cathode cylinder, and to eliminate the non-single-valuedness in the determination of the z coordinate they are split in half and the information is read out from the two sides of the chamber. Chambers 2 and 4 measure only the azimuthal coordinate. The accuracy of measuring this coordinate is $\sigma = 0.6$ mm, and $\sigma_z = 0.3$ mm.

The chambers operate on a gas mixture of 49.9% argon (Ar), 49.9% ethane (C_2H_6), and 0.2% freon ($CBrF_3$) at atmo-

TABLE V. Basic parameters of cylindrical proportional chambers of the spectrometer SINDRUM 1.

Cylindrical proportional chamber No.	1	2	3	4	5
Active length of the chamber (mm)	360	470	580	690	800
Anode diameter (mm)	128	256	384	512	640
Number of anode wires	192	384	512	768	1024
Distance between wires (mm)	2.09	2.09	2.36	2.09	1.96
Anode–cathode gap (mm)	2	2	4	4	4
Number of wires at the inner cathode	2·124	···	188	···	316
Number of wires at the outer cathode	2·132	···	196	···	324
Width of the cathode wires (mm)	2.22	···	4.44	···	4
Resistance of the cathode wires (Ω)	150	···	240	···	2
Total amount of matter (mg/cm^2)	31	31	37	49	85
Total amount of matter (r.l.$\times 10^{-6}$)	830	830	980	1280	2125

spheric pressure, and the gas multiplication is 5×10^4.

The high-voltage supply of the two-coordinate chambers (CMPCs 1, 3, and 5) of the SINDRUM 1 spectrometer operates according to a scheme different from those described for the ARES spectrometer. A positive high voltage is supplied to the anode wires. All the wires of the chamber are connected to each other through resistances of 0.5 MΩ, and the high voltage is fed through a resistance of 0.5 MΩ to each 32nd wire. The signals from the anode wires are read out via a high-voltage blocking capacitor of capacitance 500 pF. All the cathode strips are connected to ground through resistances of 0.8 MΩ, so the cathode surfaces have zero potential.

In chambers 2 and 4 a negative high voltage is fed to the solid cathode electrodes, and the anode wires are grounded through a resistance, from which the signal is also read out.

All five chambers of the spectrometer are self-supporting and have identical construction of their flanges. In chambers 1–4 the cathodes (cathodes with strips and solid cathodes) are made of aluminumized Kapton film, glued to a supporting cylinder made of the porous material Rohace11. The thickness of the supporting cylinders varied from 2 to 4 mm for chambers of different diameters. The inner and outer cathode supporting cylinders give the dominant contribution to the amount of matter quoted in Table V. The anode wires of *W*(Re) gold-plated wire 20 μm in diameter are attached to the flanges held by the inner cathode supporting cylinder.

CMPC 5 was prepared at the Laboratory for Nuclear Problems at the JINR (Ref. 78). Its cross section is shown in Fig. 17. The cathodes and supporting cylinders of this chamber are made like the analogous chambers of the ARES spectrometer. The main supporting element is the cylinder of the inner cathode. It is made from several layers of lavsan and has a total thickness of 0.41 mm. In addition, the thickness of the aluminumized cathode strips was increased from 0.1 μm to 6 μm in order to increase their stability to damage by electrochemical processes and discharges.

The construction of the apparatus for the experiment to search for muonium–antimuonium transitions was completed in 1993 and the first data-collection run was performed. The analysis of the data obtained leads to an improvement of the existing limit on the probability of the muonium–antimuonium transition by about two orders of magnitude.[79] There are plans for a second run in 1994, in which it is hoped that a limit on the transition probability at the level 10^{-11} will be attained.

3.3. Crystal sphere (PSI)

Accurate measurement of the probability for the decay $\pi^+\to\pi^0e^+\nu_e$ (pion beta decay). Accurate measurement of this decay makes it possible to rigorously verify the universality of the charged quark–lepton current and the unitarity of the Cabibbo–Kobayashi–Maskawa mixing matrix. In this experiment it is hoped that the accuracy of measuring the probability of the decay $\pi^+\to\pi^0e^+\nu_e$ can be improved from 4% to 0.5% at the first stage and to 0.2–0.3% in the next.[80] The plans are to perform the experiment at the PSI cyclotron in a π^+-meson beam of momentum ~100 MeV/*c* with stopping intensity of up to 5×10^6 π/sec. The relative probability of the decay $\pi^+\to\pi^0e^+\nu_e$ is $\sim10^{-8}$ and to measure it with a statistical accuracy of 0.2% an exposure time of about a year ($\sim2\times10^7$ sec) will be necessary.

The experiment is shown schematically in Fig. 18. Pions which have traveled through the beam counters are stopped and decay in the target. The target is surrounded by two cylindrical multiwire proportional chambers to detect charged particles. Behind the chambers is a cylindrical hodoscope made of scintillation counters with high temporal

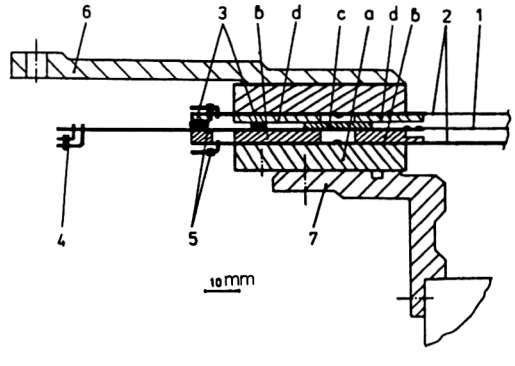

FIG. 17. Cross section of a CMPC (the rotation axis runs horizontally at the bottom). *1*—anode wires; *2*—cathode surfaces (the heavy line shows the inner cathode combined with the supporting cylinder); a, b, c, and d are elements of the chamber flange; *3*—gas gaskets; *4*—anode-wire connectors; *5*—cathode-wire connectors; *6*—element for mounting the chamber in the detector; *7*—element connecting the 5th and 4th chambers.

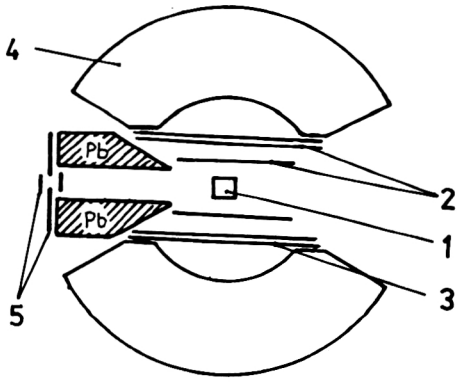

FIG. 18. Schematic depiction of the experimental setup for accurate measurement of the probability of pion beta decay. *1*—active target; *2*—CMPCs 1–2; *3*—scintillation counters; *4*—sphere of 225 CsI/CsBr crystals; *5*—beam telescope.

resolution. All this is surrounded by the main element of the setup: the shower calorimeter detecting gamma quanta from π^0-meson decay. The calorimeter has a spherical shape and consists of 225 modules of CsI–CsBr counters, each of length 12 radiation lengths. The total solid angle for detection of the setup is $0.77 \cdot 4\pi$ steradians.

The task of the cylindrical proportional chambers is to determine the charged-particle coordinates with an accuracy of <1 mm and ensure a high degree of suppression of the random coincidences of positrons from muon decay. Different versions of using hodoscopes of scintillation counters or silicon microstrip detectors for this have been studied, but when all the pros and cons were taken into account preference was given to CMPCs.

In construction the chambers will be similar to CMPC 5 of the SINDRUM spectrometer described above in Sec. 3.2. Both chambers are two-coordinate, self-supporting chambers, and their basic parameters are listed in Table VI.

Taking into account the fact that the chambers are the first object lying in the path of the detected particles, the total amount of matter in them should be of order 10^{-3} radiation lengths. This is important for the successful detection of positrons with low energies, and also for decreasing the probability of gamma conversion into electron–positron pairs in the matter of the chamber. In addition to decay of the π^0 meson from the decay of interest $\pi^+ \to \pi^0 e^+ \nu_e$, other sources of gamma quanta will be background processes such as $\pi^+ \to \mu^+ \nu\gamma$ ($\sim 1.2 \times 10^{-4}$ sec^{-1}), $\pi^+ \to e^+ \nu\gamma$ ($\sim 5.6 \times 10^{-8}$ sec^{-1}), and $\mu^+ \to e^+ \nu\bar{\nu}\gamma$ (~ 0.014 sec^{-1}), where in parentheses we give the relative decay probabilities. It is also hoped that this experiment will provide useful information about these processes.

TABLE VI. Basic parameters of cylindrical proportional chambers of the Crystal-Sphere detector.

Cylindrical proportional chamber No.	1	2
Active length of the chamber (mm)	350	540
Anode diameter (mm)	120	240
Number of anode wires	192	384
Distance between wires (mm)	1.96	1.96
Anode–cathode gap (mm)	2.5	2.5
Number of wires at the inner cathode	2·64	224
Number of wires at the outer cathode	2·64	224
Width of the cathode wires (mm)	3	2.5
Total amount of matter (mg/cm^2)	40	50
Total amount of matter (r.l.$\times 10^{-6}$)	1000	1250

CONCLUSION

There is no ideal universal detector having good values for all its parameters, and it is impossible in practice to build one. Therefore, for example, in the superdetectors used in colliding beams (DELPHI, OPAL, ATLAS...) the detection systems incorporate various types of counters, each of which is often of complex construction and has some parameter which is particularly good.

In setups at an intermediate scale it is apparently appropriate to use multi-purpose detectors like CMPCs. The examples given here illustrate the successful use of CMPCs in modern experimental physics.

[1)]In contrast to a CMPC in a cylindrical counter, the anode wire is surrounded by a cylindrical cathode.
[2)]In a chamber of this construction the second coordinate can be determined using the current-splitting method (Sec. 2.3).
[3)]Here and below this means relative to the anode.

[1] G. Charpak, Ann. Rev. Nucl. Sci. **20**, 195 (1970).
[2] G. Charpak and F. Sauli, Nucl. Instrum. Methods **162**, 405 (1979).
[3] Yu. V. Zanevskiĭ, *Wire Detectors for Elementary Particles* [in Russian] (Atomizdat, Moscow, 1978).
[4] V. D. Peshekhonov, Fiz. Elem. Chastits At. Yadra **17**, 1030 (1986) [Sov. J. Part. Nucl. **17**, 456 (1986)].
[5] G. Darbo and B. W. Heck, IEEE Trans. Nucl. Sci. **NS-34**, 227 (1987).
[6] A. Imanishi, T. Ishii, S. Kato *et al.*, Nucl. Instrum. Methods A **269**, 513 (1988).
[7] W. Blum, Nucl. Instrum. Methods **225**, 557 (1984).
[8] A. Wagner, in *Proc. of the Intern. Conf. on Instrumentation for Colliding Beam Physics*, SLAC, 1982, p. 76.
[9] R.-D. Heuer and A. Wagner, Nucl. Instrum. Methods A **265**, 11 (1988).
[10] J. Burger, L. Criegee, G. Franke *et al.*, Nucl. Instrum. Methods A **279**, 217 (1989).
[11] M. Hasemann, in *Proc. of the Intern. Conf. on Instrumentation for Colliding Beam Physics*, SLAC, 1982, p. 80.
[12] D. Rubin, J. Chapman, D. Nitz *et al.*, Nucl. Instrum. Methods **203**, 119 (1982).
[13] R. Arai, H. Boerner, N. Ishihara *et al.*, Nucl. Instrum. Methods **217**, 181 (1983).
[14] J. Adler, T. Bolton, K. Bunnell *et al.*, Nucl. Instrum. Methods A **276**, 42 (1989).
[15] P. Baringer, C. Jung, H. O. Ogren, and D. R. Rust, Nucl. Instrum. Methods A **254**, 542 (1987).
[16] W. Ash, H. R. Band, E. D. Bloom *et al.*, Nucl. Instrum. Methods A **261**, 399 (1987).
[17] A. Cordier, B. Delcourt, P. Eschstruth *et al.*, Nucl. Instrum. Methods **133**, 237 (1976).
[18] S. Egli, C. A. Meyer, P. Robmann *et al.*, Nucl. Instrum. Methods A **283**, 487 (1989).
[19] V. G. Sandukovskiĭ and V. I. Savel'ev, Fiz. Elem. Chastits At. Yadra **22**, 1347 (1991) [Sov. J. Part. Nucl. **22**, 655 (1991)].
[20] A. G. Chilingarov, Fiz. Elem. Chastits At. Yadra **23**, 785 (1992) [Sov. J. Part. Nucl. **23**, 348 (1992)].
[21] A. Oed, Nucl. Instrum. Methods A **263**, 351 (1988).
[22] F. Angelini, R. Bellazzini, L. Bosisio *et al.*, Nucl. Instrum. Methods A **314**, 450 (1992).
[23] V. N. Bychkov, I. A. Golutvin, L. G. Ignatova *et al.*, Prib. Tekh. Eksp. No. 5, 83 (1992) [Instrum. Exp. Tech.].
[24] R. Bouclier, J. J. Florent, J. Gaudaen *et al.*, Nucl. Instrum. Methods A **315**, 521 (1992).

[25] R. Bouclier, J. J. Florent, G. Million *et al.*, Preprint CERN-PPE/91-227, CERN, Geneva (1991).
[26] M. E. Rose and S. A. Korf, Phys. Rev. **59**, 850 (1941).
[27] P. M. Morse and H. Feshbach, *Methods of Theoretical Physics*, Vol. II (McGraw-Hill, New York, 1953) [Russian transl., Vol. II, IIL, Moscow, 1958], p. 231.
[28] G. Charpak, R. Bouclier, T. Bressani *et al.*, Nucl. Instrum. Methods **62**, 262 (1968).
[29] G. Charpak and F. Sauli, Ann. Rev. Nucl. Sci. **34**, 285 (1984).
[30] G. Charpak, Ann. Rev. Nucl. Sci. **20**, 195 (1970).
[31] G. A. Erskine, Nucl. Instrum. Methods **105**, 565 (1972).
[32] V. I. Tel'nov, Prib. Tekh. Eksp. No. 5, 46 (1974) [Instrum. Exp. Tech.].
[33] G. D. Alekseev, N. A. Kalinina, V. V. Kruglov, and D. M. Khazins, Prib. Tekh. Eksp. No. 4, 47 (1978) [Instrum. Exp. Tech.].
[34] F. Celani, A. Codino, F. L. Fabbri *et al.*, Nucl. Instrum. Methods **171**, 613 (1980).
[35] B. I. Khazin, Prib. Tekh. Eksp. No. 1, 64 (1981) [Instrum. Exp. Tech.].
[36] E. Epple and D. Decker, Nucl. Instrum. Methods **66**, 77 (1968).
[37] H. Aihara, J. M. Alston, D. H. Badtke *et al.*, IEEE Trans. Nucl. Sci. **NS-30**, 63 (1983).
[38] J. Jeanjean, M. Jeanjean, and R. Madaras, Nucl. Instrum. Methods **117**, 349 (1974).
[39] L. Criegee, G. Franke, U. Timm, and W. Zimmerman, in *Contrib. to the Intern. Conf. on Instrumentation for High Energy Physics*, Frascati, 1973, p. 262.
[40] G. Charpak, R. Bouclier, T. Bressani *et al.*, Nucl. Instrum. Methods **65**, 217 (1968).
[41] L. Barabash, A. M. Baranov, G. B. Bondarenko *et al.*, Nucl. Instrum. Methods A **236**, 271 (1985).
[42] V. A. Biryukov, V. G. Zinov, and F. D. Konin, Zh. Eksp. Teor. Fiz. **58**, 140 (1970) [Sov. Phys. JETP **31**, 257 (1970)].
[43] C. J. Borkowski and M. K. Kopp, IEEE Trans. Nucl. Sci. **NS-17**, 340 (1970).
[44] G. Charpak, G. Petersen, A. Policarpo, and F. Sauli, Nucl. Instrum. Methods **148**, 471 (1978).
[45] A. A. Kalinnikov, N. P. Kravchuk, A. S. Moiseenko, and A. I. Filipov, in *Proc. of the Third Intern. Meeting on Proportional and Drift Chambers*, D13-11807, JINR, Dubna (1978), p. 75 [in Russian].
[46] H. A. Bethe and J. W. Ashkin, in *Experimental Nuclear Physics*, Vol. 1, edited by E. Segré (Wiley, New York, 1953) [Russian transl., IIL, Moscow, 1955].
[47] N. B. Delone, *Bubble Chambers* (Indiana University Press, Bloomington, 1968) [Russian original, Gosatomizdat, Moscow, 1963].
[48] L. Criegee, G. Franke, E. Lohrann *et al.*, in *Contrib. to the Intern. Conf. on Instrumentation for High Energy Physics*, Frascati, 1973, p. 707.
[49] B. Sadoulet, in *Proc. of the Second Intern. Meeting on Proportional and Drift Chambers*, D13-9164, JINR, Dubna (1975), p. 55 [in Russian].
[50] N. P. Kravchuk, A. S. Moiseenko, I. Polakh, and A. I. Filippov, in *Proc. of the Second Intern. Meeting on Proportional and Drift Chambers*, D13-9164, JINR, Dubna (1975), p. 71 [in Russian].
[51] S. Ahmad, J. C. Bizot, B. Delcourt *et al.*, Nucl. Instrum. Methods **217**, 169 (1983).
[52] D. Bridges, A. Brody, A. Chen *et al.*, Physica Scripta **23**, 655 (1981).
[53] M. Kobayashi, S. Kurokawa, T. Fujitani *et al.*, Nucl. Instrum. Methods A **245**, 51 (1986).
[54] G. Aiken, D. Aston, W. Dunwoodie *et al.*, Preprint SLAC-PUB-2642, SLAC, Palo Alto (1980).
[55] G. Bologna, F. Celani, B. Caporaletti *et al.*, Nucl. Instrum. Methods **165**, 193 (1979).
[56] M. Dialinas, J. Forget, D. Geoffroy *et al.*, Preprint LAL-RT/83-14 (1983).
[57] K. Deiters, A. Donat, W. Friebel *et al.*, Nucl. Instrum. Methods A **323**, 162 (1992).
[58] E. V. Anashkin, V. M. Aulchenko, V. E. Fedorenko *et al.*, Nucl. Instrum. Methods A **323**, 178 (1992).
[59] K. Muller, H. P. Beck, K. Bosigtr *et al.*, Nucl. Instrum. Methods A **312**, 457 (1992).
[60] W. Bertl, R. Eichler, L. Felawka *et al.*, Phys. Lett. **140B**, 299 (1984).
[61] M. S. Bilen'kiĭ, P. A. Kulinich, G. V. Mitsel'makher *et al.*, Report R13-86-815, JINR, Dubna (1986) [in Russian].
[62] A. I. Filippov, A. P. Fursov, A. S. Korenchenko *et al.*, Nucl. Instrum. Methods B **17**, 441 (1986).
[63] V. A. Baranov, Yu. Vanko, A. A. Glazov *et al.*, Yad. Fiz. **53**, 1302 (1991) [Sov. J. Nucl. Phys. **53**, 802 (1991)].
[64] V. A. Baranov, A. A. Glazov, I. V. Kisel' *et al.*, Yad. Fiz. **55**, 2940 (1992) [Sov. J. Nucl. Phys. **55**, 1644 (1992)].
[65] V. A. Baranov, P. G. Evtukhovich, A. I. Filippov *et al.*, Nucl. Instrum. Methods B **17**, 438 (1986).
[66] N. P. Kravchuk, Report 1-90-575, JINR, Dubna (1990) [in Russian].
[67] A. S. Korenchenko, S. M. Korenchenko, N. P. Kravchuk *et al.*, Report 13-83-479, JINR, Dubna (1983) [in Russian].
[68] N. Chernov, A. Glazov, I. Kisel *et al.*, Comput. Phys. Commun. **74**, 217 (1993).
[69] V. A. Baranov, Yu. Banko, P. G. Evtukhovich *et al.*, in *Proc. of the Twelfth Intern. Symposium on Nuclear Electronics*, D13-85-793, JINR, Dubna (1985), p. 310 [in Russian].
[70] P. G. Evtukhovich, S. M. Korenchenko, N. A. Kuchinskiĭ, and D. A. Mzhaviya, Report R10-85-382, JINR, Dubna (1985) [in Russian].
[71] S. M. Korenchenko, USSR Author's Certificate No. 502350, OIPOTZ Bulletin, No. 5 (1976).
[72] in preparation.
[73] I. A. Baranov, S. M. Korenchenko, B. F. Kostin *et al.*, Report R1-92-131, JINR, Dubna (1992) [in Russian].
[74] K. Jungmann, B. E. Matthias, H.-J. Mundinger *et al.*, Proposal for an experiment at PSI, R89-06.1 (1989).
[75] R. Abela, J. Bagaturia, W. Bertl *et al.*, Preprint HD-PY 93/03 (1993).
[76] W. Bertl, S. Egli, R. Eichler *et al.*, Nucl. Phys. **B260**, 1 (1985).
[77] S. Egli, R. Engfer, Ch. Grab *et al.*, Phys. Lett. **175B**, 97 (1986).
[78] K. G. Nekrasov, Report R13-92-513, JINR, Dubna (1992) [in Russian].
[79] in preparation.
[80] D. Pocanic, K. A. Assamagan, D. Day *et al.*, Proposal for an experiment at PSI, R89-01.1 (1989).

Translated by Patricia A. Millard